Enhanced deuterium-tritium fusion cross sections in the presence of strong electromagnetic fields

Wenjuan Lv,[1,2] Hao Duan,[2,3,*] and Jie Liu[1,4,†]

[1]*Graduate School, China Academy of Engineering Physics, Beijing 100193, China*
[2]*Institute of Applied Physics and Computational Mathematics, Beijing 100088, China*
[3]*Laboratory of Computational Physics, Institute of Applied Physics and Computational Mathematics, Beijing 100088, China*
[4]*CAPT, HEDPS, and IFSA Collaborative Innovation Center of MoE, Peking University, Beijing 100871, China*

We investigate deuterium-tritium (DT) fusion cross sections in the presence of electromagnetic fields with high intensity and high frequency. With the help of the Kramers-Henneberger (KH) transformation, we show that the corresponding Coulomb barrier penetrability increases significantly due to the depression of the time-averaged potential barrier. As a result, we find that DT fusion cross sections can be enhanced depending effectively on a dimensionless quantity n_d, which equals the ratio of the quiver oscillation amplitude to the geometrical touching radius of the deuterium and tritium nuclei. For $n_d = 9$, we predict that the fusion cross section is almost five times the value in the absence of electromagnetic fields, which implies that the famous Lawson criterion might be relaxed to some extent.

I. INTRODUCTION

Nuclear fusion is one of the most studied issues in the fields of nuclear energy and fundamental nuclear physics because of its potential applications as a clean, effective, and sustainable energy source in the future [1]. However, controllable nuclear fusions are frustrated even in laboratory environments to achieve ignition through either magnetic confinement fusion (MCF) [2–5] or inertial confinement fusion (ICF) [6–10]. An intrinsic problem arises from the very small nuclear cross sections that greatly increase the threshold conditions of nuclear reactions and hinder the realization of controllable nuclear fusions [11–13]. Thus, seeking a possible way to increase the fusion cross section is of great interest. In the past few years, some approaches have been suggested, such as μ-meson-catalyzed [14] and spin-polarization [15,16] schemes. Unfortunately, these schemes encounter difficulties when implemented in real fusion systems. For instance, the lifetime of a μ meson is 2.2 μs, which is too short compared with the characteristic timescale of the steady fusion process in MCF and leads to an essential difficulty in controlling the injection time of a μ meson. On the other hand, the generation of a large number of μ mesons requires costly high-energy collision facilities. For the spin-polarization scheme, the main difficulty arises from the depolarizing effect induced by the frequent collisions between charged particles in fusion plasmas [17,18].

However, recent advantages in laser techniques provide an alternative scheme to manipulate nuclear processes. Since the first demonstration of laser emission from a ruby crystal (chromium-doped corundum) in 1960 [19], great improvements have been made in laser techniques. Most importantly, the advent of chirped pulse amplification (CPA) techniques [20] has enabled laser intensities up to 10^{22} W/cm^2. Laser facilities with even higher intensities are under construction in a program initiated by the European Union—namely, the Extreme Light Infrastructure (ELI) [21,22]. X-ray free-electron lasers (XFELs) are able to produce coherent light with an intensity as high as 10^{20} W/cm^2 with a wide frequency range. For example, the Linac Coherent Light Source (LCLS) can provide x-ray laser pulses with photon energies ranging from 280 eV to 11.2 keV.

Intense lasers can be applied to atomic ionization [23–25] and charged-particle acceleration [26–28] and also provide a new way for manipulating nuclear processes. It was found that intense lasers can accelerate nuclear processes by inducing resonance internal conversion [29] and increase α-decay rates [30,31] by modifying the Coulomb potential barrier. In particular, since nuclear fusion processes are mainly associated with light nuclei, we thus expect that laser manipulation will be more effective because of the relatively large charge-mass ratio compared with that in the heavy nuclei processes studied previously.

In this paper, taking the deuterium-tritium (DT) reaction as an example, we investigate nuclear fusion cross sections in the presence of electromagnetic fields and find that the DT fusion cross sections can indeed be effectively enhanced. Our results are mainly analytic, and the Kramers-Henneberger (KH) transformation [32] is exploited.

The paper is organized as follows: Section II presents our model. Section III presents discussions on the Coulomb barrier penetrability. Our main results on DT cross sections are provided in Sec. IV. Section V presents our conclusion.

---

*duan_hao@iapcm.ac.cn
†jliu@gscaep.ac.cn

II. MODEL

Nuclear fusion is commonly believed to consist of three processes [7]. First, the wave packets of two nuclei collide with each other at a probability depicted by a geometrical cross section that depends on the de Broglie wavelength. Second, the approaching nucleus tunnels through the Coulomb potential barrier. Third, the nuclei come into contact and fuse, which can be described by an astrophysical factor [33]. In the presence of electromagnetic fields, a two-body spinless model Hamiltonian of DT fusion in the velocity gauge is introduced by

$$H = \frac{(\vec{p}_1 - q_1\vec{A}(t_1, \vec{r}_1))^2}{2m_1} + \frac{(\vec{p}_2 - q_2\vec{A}(t_2, \vec{r}_2))^2}{2m_2} + V(\vec{r}_1 - \vec{r}_2), \quad (1)$$

where m_1 (m_2) and $q_1 = $ e ($q_2 = $ e) are the nuclear masses and electrical charges of deuterium (tritium) in the laboratory frame and $\vec{r}_1$ ($\vec{r}_2$) and $\vec{p}_1$ ($\vec{p}_2$) are the coordinate vectors and canonical momenta, respectively. $V(\vec{r}_1 - \vec{r}_2)$ is the two-body interaction potential between the deuterium and tritium nuclei, including the short-range attractive nuclear potential and long-range repulsive Coulomb potential, which can be given by

$$V(\vec{r}_1 - \vec{r}_2) = -\Theta\left(1 - \frac{|\vec{r}_1 - \vec{r}_2|}{r_n}\right)U_0$$
$$+ \Theta\left(\frac{|\vec{r}_1 - \vec{r}_2|}{r_n} - 1\right)\frac{e^2}{4\pi\epsilon_0|\vec{r}_1 - \vec{r}_2|}, \quad (2)$$

where the geometrical touching radius $r_n = 1.44(A_1^{\frac{1}{3}} + A_2^{\frac{1}{3}})$ fm and U_0 indicate the effective range and depth of the nuclear potential, respectively. $\Theta(x)$ is the unit step function.

In the nonrelativistic dipole approximation, by neglecting the coordinate dependence of the vector potential $\vec{A}$ and denoting $t_1 = t_2 = t$ in the nonrelativistic limit, the two-body Hamiltonian is divided into a center part $H_c = [\vec{P} - Q\vec{A}(t)]^2/2M$ and a relative part $H_r = [\vec{p} - q\vec{A}(t)]^2/2m + V(\vec{r})$ with vanishing coupling between each other $[H_c, H_r] = 0$, where $\vec{r} = \vec{r}_1 - \vec{r}_2$. The corresponding center motion and relative motion charges are $Q = 2$e and $q = (m_2 - m_1)$e$/(m_1 + m_2)$, and $M = m_1 + m_2$ and $m = m_1 m_2/(m_1 + m_2)$ are the total and reduced masses, respectively. This relative motion Hamiltonian can be reformed into

$$H_r = \frac{\vec{p}^2}{2m} + V(\vec{r}) - \frac{q}{m}\vec{A}(t) \cdot \vec{p} + \frac{q^2}{2m}\vec{A}^2(t), \quad (3)$$

The corresponding wave function in the laboratory frame is denoted $\Psi(t, \vec{r})$. By adopting the unitary KH transformation

$$\Omega(t) = \exp\left[\frac{i}{\hbar}\int_{-\infty}^t \left(-\frac{q}{m}\vec{A}(\tau) \cdot \vec{p} + \frac{q^2}{2m}\vec{A}^2(\tau)\right)d\tau\right], \quad (4)$$

The wave function under the KH framework, denoted $\Psi_{kh} = \Omega(t)\Psi$, has the same total probability as $\Psi(t, \vec{r})$ due to $\Omega^\dagger(t)\Omega(t) = 1$, and the relative motion reduces to single-body motion in the time-dependent potential $V_{kh}(t, \vec{r}_{kh}) = \Omega(t)V(\vec{r})\Omega^\dagger(t)$. The momentum operator is $\vec{p}_{kh}(t) = \Omega(t)\vec{p}\,\Omega^\dagger(t) = \vec{p}$, while the coordinate operator is

found to be $\vec{r}_{kh}(t) = \Omega(t)\vec{r}\,\Omega^\dagger(t) = \vec{r} - \vec{r}_e(t)$, which maintains the commutation relation $[r_{kh}^i(t), p_{kh}^j(t)] = i\hbar\delta^{i,j}$. $\vec{r}_e(t)$ is defined as $\hat{e}_z r_e \sin \omega t$ with $r_e = e\sqrt{2c\mu_0 I}/5m\omega^2$. Supposing that the external electromagnetic field is monochromatic and linearly polarized along the z axis, i.e., $\vec{E}(t) = \hat{e}_z E_0 \sin \omega t$, the time-dependent Schrödinger equation can be given by

$$i\hbar\frac{\partial}{\partial t}\Psi_{kh}(t, \vec{r}_{kh}) = \left(\frac{\vec{p}_{kh}^2}{2m} + V_{kh}(t, \vec{r}_{kh})\right)\Psi_{kh}(t, \vec{r}_{kh}), \quad (5)$$

where the time-dependent potential is found to be

$$V_{kh}(t, \vec{r}_{kh}) = -\Theta\left(1 - \frac{r_{kh}(t)}{r_n}\right)U_0$$
$$+ \Theta\left(\frac{r_{kh}(t)}{r_n} - 1\right)V_0\frac{r_n}{r_{kh}(t)}, \quad (6)$$

with the height of the Coulomb barrier $e^2/4\pi\epsilon_0 r_n$ denoted V_0.

For a DT collision, V_0 and r_n are approximately 0.37 MeV and 3.89 fm, respectively, while U_0 is approximately 30 to 40 MeV, i.e., two orders of magnitude larger than V_0. Equation (6) indicates that the time-dependent potential V_{kh} is just a two-body potential with a time-dependent harmonic oscillation origin $\vec{r}_e(t)$ along the polarization direction $\hat{e}_z$ with a quiver oscillation amplitude r_e. In this case, the space can be divided into two parts: the inner region denoted by a cylindrical-like region swept by the nuclear potential well, i.e., $D_{in} = \{\vec{r}\,|r_{kh}(t) \leqslant r_n, \exists\, t \in [0, 2\pi/\omega)\}$, and the outer region denoted by $D_{out} = R^3/D_{in}$. The ratio of r_e to r_n determines how external electromagnetic fields manipulate nuclei collision processes. Let us introduce a dimensionless quantity $n_d = r_e/r_n = 4.89 \times 10^{-6}\sqrt{I}/(\hbar\omega)^2$, where the units of I and $\hbar\omega$ are W/cm^2 and eV, respectively. For $r/r_n < n_d$, the Coulomb potential can be expanded according to

$$V_{kh}(t, \vec{r}) = \frac{V_0}{n_d}\frac{r_e}{r}\sum_l P_l(\cos\theta)\begin{cases}\frac{r_e^l(t)}{r^l} & |r_e(t)| \leqslant r \\ \frac{r^{l+1}}{|r_e(t)|r_e^l(t)} & r < |r_e(t)|.\end{cases} \quad (7)$$

For $r/r_n > n_d$, V_{kh} can be expanded as

$$V_{kh}(t, \vec{r}) = \frac{V_0}{n_d}\frac{r_e}{r}\sum_l P_l(\cos\theta)\frac{r_e^l(t)}{r^l}, \quad (8)$$

where θ is the inclination angle of $\vec{r}$. By noticing Eqs. (7) and (8), the external fields can remarkably reduce the height of the Coulomb barrier via the factor V_0/n_d and yield an enhanced tunneling probability for $n_d > 1$.

III. PENETRABILITY

In the nonrelativistic limit, the corresponding quiver velocity of the incident nucleus should be much less than the vacuum light speed, i.e., $\eta = e\sqrt{2c\mu_0 I}/5m\omega c \ll 1$. On the other hand, the laser intensity I is not allowed to exceed the Schwinger limit $I_0 = m_e^4 c^5/\mu_0 e^2\hbar^2$ [34], and the electromagnetic field frequency must be less than $\omega^* = m_e c^2/\hbar$ to avoid the $\gamma + \gamma^* \to e + e^+$ process. All of the above limitations are shown in the parameter diagram of Fig. 1, in which we also plot the typical parameters of various laser facilities at the present time.
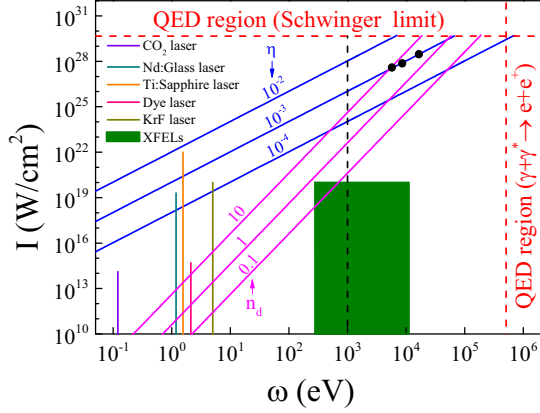
FIG. 1. Phase diagram for the laser parameters of currently achievable lasers, e.g., a CO_2 laser with a peak intensity of 1.30×10^{14} W/cm^2 and a frequency of 0.12 eV [35]; a Nd:glass laser with a peak intensity of 2.00×10^{19} W/cm^2 and a frequency of 1.18 eV [36]; a Ti:sapphire laser with a peak intensity of 1.00×10^{22} W/cm^2 and a frequency of 1.55 eV [37]; a dye laser with a peak intensity of 5.00×10^{14} W/cm^2 and a frequency of 2.12 eV [38]; a KrF laser with a peak intensity of 1.00×10^{20} W/cm^2 and a frequency of 5.00 eV [39]; and XFELs with a peak intensity of 1.00×10^{20} W/cm^2 and variable frequencies from 280 eV to 11.2 keV [40,41]. The horizontal red dashed line and the vertical red dashed line represent the Schwinger limit of the laser intensity, 4.6×10^{29} W/cm^2, and the QED limit of the laser frequency, 0.51 MeV, respectively. The vertical dashed black line represents a laser frequency of 1 keV, above which the field period is much smaller than the characteristic nuclear collision time so that the time-averaged scheme in the KH framework is expected to be valid. The solid blue lines denote $\eta = 10^{-2}$, 10^{-3}, and 10^{-4}. The solid pink lines denote $n_d = 0.1$, 1, and 10. The black points are three typical laser parameters for our following detailed discussion: the corresponding dimensionless parameters are $n_d = 3$, 6, and 9, and the laser parameters are 5.36×10^3 eV, 3.37×10^{27} W/cm^2; 8.46×10^3 eV, 7.62×10^{27} W/cm^2; and 1.69×10^4 eV, 3.05×10^{28} W/cm^2, respectively.

Usually, the collision energies of a typical DT fusion process are approximately tens of keV, and the corresponding characteristic collision time T_0 is approximately several femtoseconds. When the characteristic collision time is much longer than the field period, i.e., $T_0 \gg 2\pi/\omega$, the time-dependent operator $\vec{r}_{kh}(t)$ can be well approximated by its time-averaged value $\overline{\vec{r}_{kh}(t)} = \vec{r}$, indicating that the incident nucleus feels a time-averaged potential $\overline{V_{kh}(t, \vec{r})} = V_{eff}(\vec{r})$. We choose 1 keV as the threshold of the laser frequency beyond which the average scheme is valid.

In the region of D_{in}, V_{eff} can be approximated as $-U_0$ due to the fact $V_0/U_0 \sim 10^{-2}$. In the region of D_{out}, the odd-l terms of the Coulomb potential cancel in the duration of an oscillation, and only even-l terms remain. The time-averaged potential can be given by

$$V_{eff}(\vec{r}) = \begin{cases} -U_0, & \vec{r} \in D_{in} \\ \frac{V_0}{n_d} \sum_{l \in even} P_l(\cos\theta) V_l(r), & \vec{r} \in D_{out}. \end{cases} \quad (9)$$
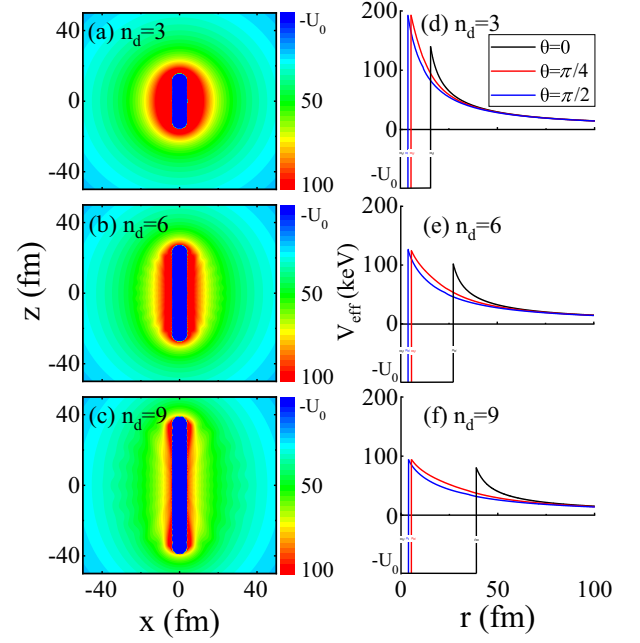
FIG. 2. The effective potential has rotational symmetry with respect to the z axis. (a)–(c) Contour plots on x-z section of the effective potential for $n_d = 3$, 6, and 9, respectively. The blue areas represent the section ($y = 0$) of inner region D_{in} where the potential value is approximately $-U_0$. D_{in} consists of a cylindrical region and two hemispheres at the top and bottom ends. The length of the cylinder is $2r_e$, and the radius of both the cylinder and the hemisphere is r_n. (d)–(f) V_{eff} for different inclination angles θ with respect to varied $n_d = r_e/r_n$.

The corresponding partial-wave potential V_l in the region of D_{out} is found to be

$$\begin{aligned} V_l(r) = \frac{1}{\pi} \sum_{i=1}^{\frac{l}{2}} & \left[-\left(\frac{r}{r_e}\right)^{2i-l-2} + \left(\frac{r}{r_e}\right)^{-2i+l} \right] \\ & \times \sqrt{1 - \left(\frac{r}{r_e}\right)^2} \frac{\Gamma\left(\frac{l+1}{2}\right)\Gamma(i)}{\Gamma\left(\frac{l}{2}+1\right)\Gamma\left(i+\frac{1}{2}\right)} \\ & + \frac{1}{\pi}\left(\frac{r}{r_e}\right)^{-l-1} \frac{2\Gamma\left(\frac{l+1}{2}\right)}{\sqrt{\pi}\Gamma\left(\frac{l}{2}+1\right)} \arcsin\frac{r}{r_e} \\ & - \frac{1}{\pi}\left(\frac{r}{r_e}\right)^{l} \frac{2\Gamma\left(\frac{l+1}{2}\right)}{\sqrt{\pi}\Gamma\left(\frac{l}{2}+1\right)} \ln\tan\frac{\arcsin\frac{r}{r_e}}{2} \end{aligned}$$
$$(10)$$

for $r/r_n \leqslant n_d$, and

$$V_l(r) = \left(\frac{r}{r_e}\right)^{-l-1} \frac{\Gamma\left(\frac{l+1}{2}\right)}{\sqrt{\pi}\Gamma\left(\frac{l}{2}+1\right)} \quad (11)$$

for $r/r_n > n_d$. The corresponding time-averaged potential V_{eff} for $n_d = 3$, 6, and 9 is shown in Fig. 2.

Using the Wenzel-Kramers-Brillouin approximation [42], the penetrability through the Coulomb barrier at the collision
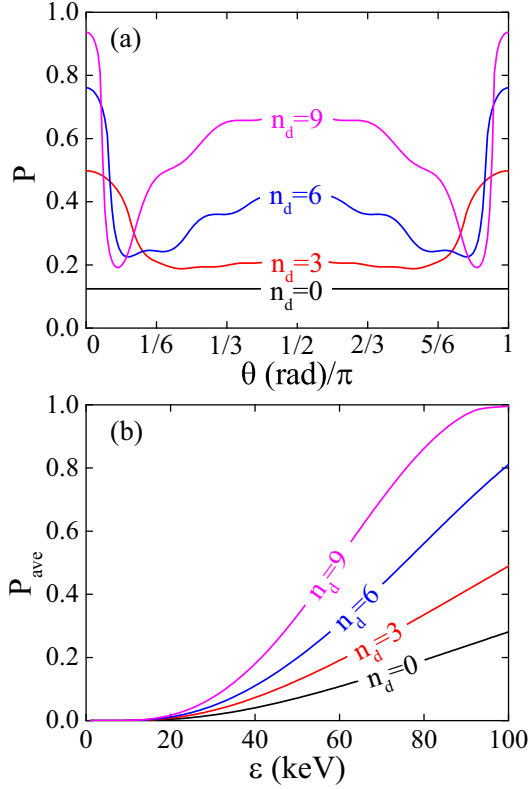
FIG. 3. (a) Angle-dependent penetrability for collision energy of $\epsilon = 64$ keV. (b) Average penetrability versus collision energy.

energy ϵ along the direction $\hat{r}$ can be given by

$$P(\theta; \epsilon, n_{\mathrm{d}}) = \exp\left(-\frac{2}{\hbar} \int_{r_{\mathrm{in}}}^{r_{\mathrm{out}}} \sqrt{2m[V_{\mathrm{eff}}(\vec{r}) - \epsilon]}\, dr\right), \quad (12)$$

where r_{in} and r_{out} are the inner and outer turning points, respectively. Due to the symmetry of the Hamiltonian, the penetrability is independent of the azimuth ϕ. The penetrability depends explicitly on the incident energy, the inclination angle θ, and the dimensionless parameter n_{d}.

The angle-dependent penetrability can be readily obtained by numerically calculating Eq. (12), and the results are plotted in Fig. 3(a). The angle-dependent penetrabilities exhibit an interesting double-hollow structure with some small oscillations. This indicates that the penetrability can reach local maxima in the directions parallel and perpendicular to the laser polarization direction, i.e., $\theta = 0$, π and $\theta = \pi/2$. This is due to the distortion of the effective potential in both its peak and width in the presence of strong fields, as shown in Fig. 2. Along the polarization direction $\hat{e}_z$ of $\theta = 0$, π, both the peak value and the barrier width are found to decrease significantly. At $\theta = \pi/2$, the tunneling is along the large potential gradient direction that can lead to the second local maximum probability. The hollows correspond to the minimum penetrability, and their positions are approximately θ^* and $\pi - \theta^*$, with $\theta^* = 2\arctan(r_{\mathrm{n}}/r_{\mathrm{e}}) = 2\arctan(1/n_{\mathrm{d}})$. This can be understood by observing the geometric character of the contour plots of the average potentials as shown in

Figs. 2(a)–2(c). The small oscillations arise from the high-order Legendre terms.

The emergence of the local maximum peak at $\theta = \pi/2$ is analogous to what occurs in the α-decay process discussed by Delion and Ghinescu [30]. However, along the polarization direction of $\theta = 0$, π, their calculated probability is a local minimum instead. In the α-decay model of Ref. [30], the oscillations of the nuclear potential in the external fields are ignored. This local maximum in the direction perpendicular to the laser polarization does not emerge in the more recent work for α decay [31], in which the validity of the time-average scheme in the KH coordinate is questioned and instead the length gauge is exploited.

The angle-averaged penetrability can be obtained by taking an average over the 4π solid angle; that is,

$$P_{\mathrm{ave}}(\epsilon; n_{\mathrm{d}}) = \frac{1}{2} \int_0^{\pi} P(\theta; \epsilon, n_{\mathrm{d}}) \sin\theta\, d\theta. \quad (13)$$

The penetrability versus the collision energy for different n_{d} values is shown in Fig. 3(b), indicating that the penetrability increases significantly with respect to the dimensionless parameter n_{d}.

IV. ENHANCED DEUTERIUM-TRITIUM FUSION CROSS SECTIONS

As mentioned above, DT nuclear fusion consists of three processes, and the nuclear fusion cross sections are usually given in a phenomenological Gamow form as a product of three terms:

$$\sigma(\epsilon) = \frac{S(\epsilon)}{\epsilon} \exp\left(-\sqrt{\frac{\epsilon_{\mathrm{G}}}{\epsilon}}\right), \quad (14)$$

where the term $1/\epsilon$ is the geometrical cross section, which is proportional to the square of the de Broglie wavelength of the relative motion. In addition, the term $\exp(-\sqrt{\epsilon_{\mathrm{G}}/\epsilon})$ is the tunneling probability through the Coulomb potential barrier, which holds as far as $\epsilon \ll \epsilon_{\mathrm{G}}$. For DT fusion, the Gamow energy factor is $\epsilon_{\mathrm{G}} = (e^2 \sqrt{2m}/4\hbar\epsilon_0)^2 = 1.18$ MeV, so Eq. (14) can be used for collision energies of $\epsilon < 100$ keV. S, which is a weakly varying function of collision energy, is
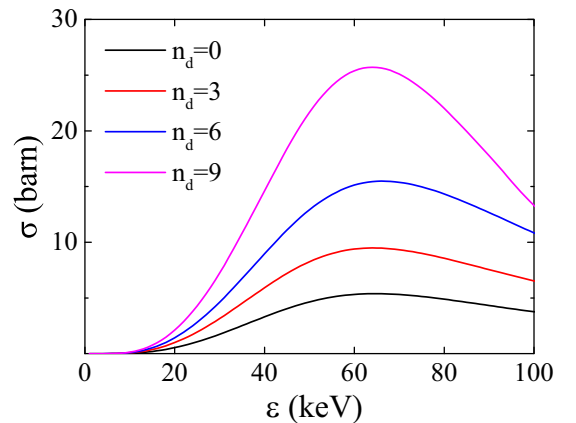
FIG. 4. Fusion cross sections versus collision energy for $n_{\mathrm{d}} = 0$, 3, 6, and 9.

the so-called astrophysical factor that describes the nuclear physics within the nuclear potential effective range. In the absence of external electromagnetic fields, the S factor can be given by a fitting function

$$S(\epsilon) = a + \frac{b}{\pi} \frac{d}{4(\epsilon - c)^2 + d^2}, \qquad (15)$$

where the parameters are found to be $a = 118.8$ keV barn, $b = 8.647 \times 10^5$ keV^2 barn, $c = 45.05$ keV, and $d = 86.76$ keV.

In the presence of external fields, the astrophysical S factor can still be described by Eq. (15), and the probability of a wave-packet collision $1/\epsilon$ also remains unchanged, while the Coulomb barrier penetrability should be replaced by P_{ave}. As shown in Fig. 4, the fusion cross sections σ have been significantly enhanced with increasing n_d, which indicates that high-intensity and high-frequency electromagnetic fields can effectively increase the DT fusion cross sections.

V. CONCLUSION

In summary, we show that DT fusion cross sections can be enhanced depending on a dimensionless parameter n_d

in the presence of high-intensity and high-frequency electromagnetic fields. For a collision energy of 64 keV and when n_d is equal to 9, the penetrability is approximately 4.92 times as large, and the fusion cross sections can be enhanced to 25.7 barns, which is approximately 4.77 times that of the field-free case. In this situation we approximately estimate that the averaged fusion reactivity can be multiplied approximately five times so that the Lawson criterion [43] might be reduced to one fifth of the value in the absence of electromagnetic fields. However, when calculating energy balance, we ignore the power needed to create and maintain the superstrong electromagnetic fields. This issue will be discussed in detail in future work. On the other hand, this work focuses on the high-frequency limit. Extending these discussions to the situation of relatively low frequency is ongoing.

[1] E. G. Ade lberger, S. M. Austin, J. N. Bahcall, A. B. Balantenkin, G. Bogaert, L. S. Brown *et al.*, Rev. Mod. Phys. **70**, 1265 (1998).

[2] F. L. Hinton and R. D. Hazeltine, Rev. Mod. Phys. **48**, 239 (1976).

[3] J. Sheffield, Rev. Mod. Phys. **66**, 1015 (1994).

[4] J. Ongena, R. Koch, R. Wolf, and H. Zohm, Nat. Phys. **12**, 398 (2016).

[5] http://www-fusion-magnetique.cea.fr/gb/index.html.

[6] J. Nuckolls, L. Wood, A. Thiessen, and G. Zimmerman, Nature (London) **239**, 139 (1972).

[7] S. Atzeni and J. Meyer-ter-Vehn, *Inertial Fusion Beam Plasma Interaction, Hydrodynamics, Dense Plasma Physics* (Clarendon Press, Oxford, 2003).

[8] J. D. Lindl, P. Amendt, R. L. Berger *et al.*, Phys. Plasmas **11**, 339 (2004).

[9] O. A. Hurricane, D. A. Callahan, D. T. Casey, P. M. Celliers *et al.*, Nature (London) **506**, 343 (2014).

[10] R. Betti and O. A. Hurricane, Nat. Phys. **12**, 435 (2016).

[11] B. H. Flowers, Proc. R. Soc. London, Ser. A **204**, 503 (1951).

[12] H. V. Argo, R. F. Taschek, H. M. Agnew, A. Hemmendinger, and W. T. Leland, Phys. Rev. **87**, 612 (1952).

[13] H. S. Bosch and G. M. Hale, Nucl. Fusion **32**, 611 (1992).

[14] L. I. Ponomarev, Contemp. Phys. **31**, 219 (1990).

[15] R. M. Kulsrud, H. P. Furth, E. J. Valeo, and M. Goldhaber, Phys. Rev. Lett. **49**, 1248 (1982).

[16] G. Hupin, S. Quaglioni, and P. Navrátil, Nat. Commun. **10**, 351 (2019).

[17] A. B. Balantekin and N. Takigawa, Rev. Mod. Phys. **70**, 77 (1997).

[18] Y. A. Thalmann, R. Jacot-Guillarmod, F. Mulhauser, L. A. Schaller, L. Schellenberg, H. Schneuwly, S. Tresch, and A. Werthmuller, Phys. Rev. A **57**, 1713 (1998).

[19] T. H. Maiman, Nature (London) **187**, 493 (1960).

[20] D. Strickland and G. Mourou, Opt. Commun. **56**, 219 (1985).

[21] http://www.eli-np.ro.

[22] http://www.eli-hu.hu.

[23] C. J. Joachain, N. J. Kylstra, and R. M. Potvliege, *Atoms in Intense Laser Fields* (Cambridge University Press, Cambridge, 2012).

[24] J. Liu, *Classical Trajectory Perspective of Atomic Ionization in Strong Laser Fields* (Springer, Berlin, Heidelberg, 2014).

[25] K. Mima, J. Fuchs, T. Taguchi *et al.*, Matter Radiat. Extrem. **3**, 127 (2018).

[26] S. P. D. Mangles, C. D. Murphy, Z. Najmudin *et al.*, Nature (London) **431**, 535 (2004).

[27] C. G. R. Geddes, Cs. Toth, J. van Tilborg *et al.*, Nature (London) **431**, 538 (2004).

[28] J. Faure, Y. Glinec, A. Pukhov *et al.*, Nature (London) **431**, 541 (2004).

[29] F. F. Karpeshin, Phys. Part. Nucl. **37**, 284 (2006).

[30] D. S. Delion and S. A. Ghinescu, Phys. Rev. Lett. **119**, 202501 (2017).

[31] J. T. Qi, T. Li, R. H. Xu, L. B. Fu, and X. Wang, Phys. Rev. C **99**, 044610 (2019).

[32] W. C. Henneberger, Phys. Rev. Lett. **21**, 838 (1968).

[33] G. Gamow, Eur. Phys. J. A **51**, 204 (1928).

[34] J. Schwinger, Phys. Rev. **82**, 664 (1951).

[35] H. Daido, F. Miki, K. Mima, M. Fujita, K. Sawai, H. Fujita, Y. Kitagawa, S. Nakai, and C. Yamanaka, Phys. Rev. Lett. **56**, 846 (1986).

[36] J. Badziak, S. Jabioński, P. Parys *et al.*, Laser Part. Beams **28**, 575 (2010).

[37] S. W. Bahk, P. Rousseau, T. A. Planchon *et al.*, Opt. Lett. **29**, 2837 (2004).

[38] M. D. Perry, O. L. Landen, A. Szöke, and E. M. Campbell, Phys. Rev. A **37**, 747 (1988).

[39] R. Sadighi-Bonabi, H. Hora, Z. Riazi, E. Yazdani, and S. K. Sadighi, Laser Part. Beams **28**, 101 (2010).

[40] https://lcls.slac.stanford.edu.

[41] P. H. Bucksbaum and N. Berrah, Phys. Today **68**(7), 26 (2015).

[42] L. D. Landau and E. M. Lifshitz, *Quantum Mechanics Non-Relativistic Theory* (Pergamon Press London-Paris, 1958).

[43] J. D. Lawson, Proc. Phys. Soc., London, Sect. B **70**, 6 (1957).